Article

Discovery Medicine 2026; 38(210): 2317–2327
https://doi.org/10.24976/Discov.Med.202638210.181

Unlocking Bone Health: How Syringin Inhibits Osteoclasts via PTGS1 in Postmenopausal Osteoporosis

Qi Zhang[1,*], Yanhua Yang[2], Jinhua Hu[3]

[1]Department of Pharmacy, Changzhou No.7 People's Hospital (Changzhou Geriatric Hospital Affiliated to Soochow University), 213000 Changzhou, Jiangsu, China
[2]Department of Science and Education, Changzhou No.7 People's Hospital (Changzhou Geriatric Hospital Affiliated to Soochow University), 213000 Changzhou, Jiangsu, China
[3]Department of Pharmacy, Shanghai Fourth People's Hospital Affiliated to Tongji University, 200434 Shanghai, China
*Correspondence: Qizhang_4562@163.com (Qi Zhang)
Submitted: 13 April 2026 Revised: 22 May 2026 Accepted: 23 June 2026 Published: 23 July 2026

Background: Postmenopausal osteoporosis (PMOP) is a common metabolic bone disease resulting from excessive osteoclast activity, characterized by reduced bone mineral density and increased fracture risk. Syringin (SRG), a natural phenylpropanoid glycoside, has shown potential anti-osteoporotic effects; however, its molecular mechanism remains unclear. This study investigated whether SRG inhibits osteoclast differentiation through regulating prostaglandin-endoperoxide synthase 1 (PTGS1).
Methods: RAW 264.7 cells were induced with receptor activator of nuclear factor-κB ligand (RANKL) and treated with SRG at 0, 2.5, 5, and 10 μM. Osteoclast differentiation was evaluated by tartrate-resistant acid phosphatase (TRAP) staining and F-actin ring staining. The mRNA levels of cathepsin K (*CTSK*), matrix metalloproteinase-9 (*Mmp9*), and nuclear factor of activated T cells 1 (*NFATc1*) were measured by quantitative reverse transcription polymerase chain reaction (qRT-PCR), and PTGS1 (also known as COX1) protein expression was detected by Western Blot (WB). PTGS1 expression was regulated to assess its role in SRG-mediated effects. *In vivo*, an ovariectomized (OVX) rat model was established, and SRG was administered orally at 25 and 50 mg/kg for 8 weeks. Bone mineral density, serum biomarkers (TRAP, alkaline phosphatase [ALP], alanine aminotransferase [ALT], aspartate aminotransferase [AST]), and femoral histopathology were analyzed.
Results: SRG significantly inhibited RANKL-induced osteoclast differentiation, accompanied by reduced expression of PTGS1, CTSK, *Mmp9* and NFATc1 ($p < 0.01$). PTGS1 overexpression partially reversed these inhibitory effects of SRG ($p < 0.05$), supporting the involvement of PTGS1 in SRG-mediated regulation of osteoclast differentiation. In the OVX-induced PMOP rat model, SRG treatment increased femoral density ($p < 0.01$), reduced serum levels of TRAP, ALP and AST ($p < 0.05$), and improved bone tissue structure.
Conclusion: SRG effectively inhibits osteoclast differentiation and mitigates OVX-induced osteoporosis via PTGS1, positioning it as a potential candidate compound for PMOP.

Keywords: postmenopausal osteoporosis; syringin; osteoclast differentiation; prostaglandin-endoperoxide synthase 1

Introduction

Osteoporosis, characterized by reduced bone density and impaired bone microarchitecture, is a chronic condition that greatly increases the risk of fractures [1]. Postmenopausal osteoporosis (PMOP) represents the most prevalent form of osteoporosis in postmenopausal women, which is highly attributed to the sudden drop in estrogen levels following menopause [2]. Estrogen plays a crucial role in maintaining bone metabolism, and its deficiency accelerates bone resorption and contributes to the onset and progression of osteoporosis. The pathophysiological mechanisms of osteoporosis primarily involve an imbalance between osteoclasts and osteoblasts during the bone remodeling process [3]. Under normal conditions, osteoclasts are responsible for bone resorption, while osteoblasts facilitate bone formation. However, the lack of estrogen postmenopause significantly enhances osteoclast activity, accelerating bone resorption and ultimately diminishing bone density [4]. Clinically, patients often exhibit symptoms such as bone pain, fractures, and decreased height, severely impacting their quality of life [5]. Osteoclasts are central to the pathogenesis of PMOP, as they secrete protons and proteolytic enzymes that dissolve bone minerals and organic matrix, thereby facilitating bone resorption [6]. Furthermore, elevated inflammatory factors (such as interleukin-6 and tumor necrosis factor-alpha) in the bone microenvironment, along with oxidative stress-related cellular damage, further promote osteoclast proliferation and activity, exacerbating bone loss [7]. Osteoclasts are also essential for maintaining bone homeostasis, and their dysfunction directly impacts the onset of osteoporosis. Therefore, thera-

Copyright: © 2026 The Author(s). Published by Discovery Medicine. This is an open access article under the CC BY 4.0 license.
Note: *Discovery Medicine* stays neutral with regard to jurisdictional claims in published maps and institutional affiliations.

peutic strategies targeting osteoclasts hold promise for improving bone density and preventing fractures in PMOP patients.

Syringin (SRG) is a naturally occurring plant-derived substance that exhibits a wide range of biological activities, including anti-inflammatory, anticancer, and antioxidant properties [8]. Recent studies have suggested that SRG may be beneficial for both the treatment and prevention of osteoporosis [9], but its underlying mechanisms of action remain unclear and warrant further investigation. Network pharmacology analysis was performed, and identified prostaglandin-endoperoxide synthase 1 (PTGS1) as a potential target of SRG (**Supplementary Table 1**), providing insights into the potential mechanisms underlying its anti-osteoporotic effects. Previous research has shown that PTGS1 expression is significantly elevated in osteoclasts treated with lipopolysaccharide (LPS), highlighting its important role in bone metabolism [10]. The synthesis of prostaglandin E2 (PGE2) catalyzed by PTGS1 is closely linked to bone remodeling, as PGE2 can influence osteoclast activity by regulating the expression of matrix metalloproteinase-9 (MMP9) [11]. Notably, MMP9 has been considered a key regulator of osteoclast invasion activity, with changes in its expression levels directly affecting the incidence of osteoporosis [12]. In this study, we systematically investigated the effects of SRG on PMOP, with particular emphasis on its modulation of PTGS1.

Materials and Methods

Network Pharmacology

The detailed network pharmacology methods are described in the **Supplementary Methods**.

Animal Ethics

A total of 40 female Sprague-Dawley (SD) rats (12 weeks old, approximately 250 g) were provided by Hangzhou Medical College (China). All procedures involving animals were conducted in accordance with protocols approved by the Animal Ethics Committee of Zhejiang Provincial Animal Center (Approval No. ZJCLA-IACUC-20011001). Animals were maintained under controlled environmental conditions (12-h light/dark cycle, 22 ± 2 °C, relative humidity of 55 ± 10%) with free access to food and water. To reduce physiological stress-caused changes, the animals were allowed to acclimate for at least five days prior to the tests.

Osteoclast Induction

The murine macrophage cell line RAW 264.7 (CL-0190, Procell, Wuhan, China) was verified to be free of mycoplasma contamination and authenticated using short tandem repeat (STR) analysis. Cells were cultivated at 37 °C in a humidified atmosphere with 5% CO_2 in α-Minimum Essential Medium (αMEM; DBM0103A, Seebio, Shanghai, China) supplemented with 10% fetal bovine serum (FBS; A5256701, Thermo Fisher, Shanghai, China), 2-4 mM L-glutamine and penicillin-streptomycin (100 U/mL; 10378016, Thermo Fisher, Shanghai, China). Osteoclastogenesis was induced by treating RAW 264.7 cells with 30 ng/mL RANKL for 5 days [13]. Successful osteoclast differentiation was confirmed by tartrate-resistant acid phosphatase (TRAP) staining.

Cell Treatment

RAW 264.7 cells were divided into four groups based on SRG concentration: 0, 2.5, 5, and 10 μM. SRG (HY-N0824, MCE, NJ, USA; purity >99%) was used in all experiments. Osteoclast differentiation was induced with RANKL (30 ng/mL) for 5 days in the presence or absence of SRG (0, 2.5, 5, 10 μM) [14]. The PTGS1 overexpression vector (pRP [Exp]-EGFP-CMV>mPtgs1 [NM_008969.4]) and negative control (NC; pRP [Exp]-EGFP-CMV>ORF_Stuffer) were constructed by VectorBuilder (Guangzhou, China). Cells in the SRG+NC and SRG+PTGS1 groups were transfected with 10 nM plasmids using Lipofectamine 2000 (11668019, Invitrogen, CA, USA) in 6-well plates (1×10^5 cells/well; FCP060, Beyotime, Shanghai, China) and incubated for 48 h at 37 °C. Transfection efficiency was assessed by quantitative reverse transcription polymerase chain reaction (qRT-PCR) analysis. Following transfection, cells were treated with RANKL (30 ng/mL) and SRG (5 μM) for another 5 days.

F-Actin Ring Staining

RAW 264.7 cells were treated with SRG and RANKL as described above. After 5 days of incubation, cells were fixed with 4% paraformaldehyde (P0099, Beyotime, Shanghai, China) for 30 min, permeabilized with 0.1% Triton X-100 for 15 min, and stained with phalloidin-FITC (1:200 in 1% BSA, ab235137, Abcam, Cambridge, UK) for 30 min at room temperature in the dark. Nuclei were counterstained with DAPI (C0065, Solarbio, Beijing, China) for 5 min. Fluorescence images were captured using an IX71 microscope (Olympus, Tokyo, Japan).

TRAP Staining

4% paraformaldehyde was utilized to treat RAW 264.7 cells. As directed by the manufacturer, a TRAP kit (BB-4421, Beibo Bio, Nanjing, China) was used for TRAP staining. Reddish-purple cytoplasmic precipitates with negative cell nuclei were indicative of positive TRAP staining. Osteoclasts were characterized as multinucleated TRAP-positive cells with three or more nuclei. TRAP-positive multinucleated cells were observed under an optical microscope (200×, Micromed, Shenzhen, China) and quantitatively analyzed using ImageJ software (version 1.54, National Institutes of Health, MD, USA).

qRT-PCR

RAW 264.7 cells were extracted with TRIzol reagent (R0016, Beyotime, Shanghai, China) to extract total RNA, followed by RNA concentration determination using a spectrophotometer (GE Healthcare, CA, USA). The Transcriptor First Strand cDNA Synthesis Kit (04379012001, Roche, CA, USA) was employed to reverse-transcribe 1.0 µg of total RNA into first-strand cDNA, yielding a final volume of 20 µL. qRT-PCR was performed on an ABI 7500 Real-Time PCR System (CA, USA) using the SYBR Green PCR Master Mix (4344463, Thermo Fisher, CA, USA). Gene expression levels of cathepsin K (*CTSK*), *Mmp9*, nuclear factor of activated T cells 1 (*NFATc1*), and glyceraldehyde-3-phosphate dehydrogenase (*GAPDH*; internal control) were determined using the $2^{-\Delta\Delta Ct}$ technique [15]. **Supplementary Table 2** lists the primer sequences (Tsingke, Beijing, China).

Western Blot (WB) Analysis

As per the manufacturer's instructions, radioimmunoprecipitation assay (RIPA) lysis buffer (P0013, Beyotime, Shanghai, China) was used to extract total protein from RAW 264.7 cells. The bicinchoninic acid (BCA) test was utilized to determine total protein in the supernatant (P0009, Beyotime, Shanghai, China). Proteins were transferred to polyvinylidene difluoride membranes (FFP24, Beyotime, Shanghai, China) after sodium dodecyl sulfate-polyacrylamide gel electrophoresis (P0690, Beyotime, Shanghai, China). Following blocking with 5% non-fat milk, membranes were incubated with primary antibodies anti-COX1 (69 kDa, ab109025, Abcam, Cambridge, UK), anti-NFAT2 (100 kDa, ab25916, Abcam, Cambridge, UK) and loading control anti-GAPDH (36 kDa, ab8245, Abcam, Cambridge, UK) overnight at 4 °C. Next, membranes were incubated with secondary antibodies (ab6721, ab205719, Abcam, Cambridge, UK) for 60 min at room temperature. Protein bands were visualized using an enhanced chemiluminescence detection kit (KGC4902, Keygene, Jiangsu, China). Band intensities were detected using ImageJ software (version 1.54, National Institutes of Health, MD, USA).

Ovariectomy (OVX)-Induced Osteoporosis Model and Drug Treatment

SD rats were randomly assigned to Sham, OVX, 17β-estradiol (E_2), SRG-low (L), and SRG-high (H) groups (n = 8 per group). For PMOP modeling, rats in all other groups underwent bilateral ovariectomy under anesthesia with 4% isoflurane (26675-46-7, Shenggong Biological, Shanghai, China) [16] delivered using a small-animal anesthesia machine (RWD510, RWD Life Science, Shenzhen, China) equipped with an isoflurane vaporizer. Throughout the surgical operation, 2% isoflurane was administered via a nose cone to maintain anesthesia. Rats in the Sham group received the same surgical procedure without ovariectomy. Drug administration began one day after surgery. The E_2 group received oral E_2 at 100 µg/kg (E8875, Merck, CA, USA) once daily, dissolved in 0.5% Carboxymethyl Cellulose Sodium (CMC-Na) as the vehicle [17]. SRG was administered orally at doses of 25 mg/kg and 50 mg/kg in the SRG-L and SRG-H groups, respectively [14]. The Sham and OVX groups received an equal amount of distilled water (Millipore, Darmstadt, Germany). All treatments were performed once daily at a fixed time each morning for 8 consecutive weeks. Body weight was recorded weekly throughout the experimental period. At the end of the treatment period, rats were anesthetized with sodium pentobarbital (80 mg/kg; P3761, Sigma-Aldrich, USA). Blood samples were then collected by left ventricular puncture, followed by euthanasia via cervical dislocation. Serum was separated by centrifugation and stored at –80 °C. The femora and uteri were harvested and weighed. The femora were subsequently fixed overnight in 10% neutral buffered formalin at room temperature (NBF; BL388A, Biosharp, Hefei, China).

Bone Density Measurement

The collected femora were placed in conical tubes (84031ES03, YEASEN, Shanghai, China) with distilled water and subjected to vacuum in a machine (Eppendorf, Hamburg, Germany) for 90 min to remove air. Using gauze, extra water was carefully extracted from the femora before being weighed. After that, the femora were moved to a fresh conical tube and weighed again in distilled water. As previously mentioned, Archimedes' principle (g/cm^3 of bone volume) was used to determine bone density [17].

TRAP Activity Assay

According to the manufacturer's instructions, a TRAP assay kit (P0332, Beyotime, Shanghai, China) was exploited to quantify TRAP activity in rat serum. Using a microplate reader (Molecular Devices, CA, USA), absorbance was measured at 405 nm.

Enzyme-Linked Immunosorbent Assay (ELISA)

Commercial assay kits were used to determine the serum levels of alkaline phosphatase (ALP; RX301651R, Ruixin Biotech, Quanzhou, China), aspartate aminotransferase (AST; ASTHB302-Ra, Hnybio, Shanghai, China), and alanine aminotransferase (ALT; RX301398R, Ruixin Biotech, Quanzhou, China) according to the manufacturers' instructions. Serum samples were appropriately diluted to ensure that all measurements fell within the linear detection range of the standard curve. Absorbance was measured at 450 nm using a microplate reader. All standard curves demonstrated good linearity with correlation coefficients (R^2) greater than 0.99.

Histological Staining

Femurs were fixed in 10% NBF, decalcified in 10% ethylenediaminetetraacetic acid (EDTA; 60-00-4, Sangon Biotech, Shanghai, China) for three weeks, embedded in paraffin (8002-74-2, Sangon Biotech, Shanghai, China), and cut into slices (5 μm thick). A staining procedure, using hematoxylin and eosin (H&E; MM1013, Maokangbio, Shanghai, China), was performed to evaluate histological alterations. Slices were stained with TRAP using the TRAP kit (PMK0467, Bioprimacy, Wuhan, China) as described above and then counterstained with methyl green (MS4035, Maokangbio, Shanghai, China) to detect osteoclasts (nuclei appear green and cytoplasmic precipitate appears reddish-purple). The stained tissues were examined under an optical microscope (200×). Trabecular area was quantified using ImageJ software (version 1.54, National Institutes of Health, MD, USA).

Immunohistochemistry (IHC) Staining

Femurs encapsulated in paraffin were cut into slices (5 μm thick) and subjected to antigen retrieval using citrate buffer (C2488, Sigma-Aldrich, CA, USA). The slices were then blocked for 1 h at room temperature with 5% bovine serum albumin (BSA, ST025, Beyotime, Shanghai, China). Slices were then incubated with primary antibody against NFATc1 (MA3-024, Thermo Fisher, CA, USA) overnight at 4 °C. After thorough washing with phosphate-buffered saline (C0221A, Beyotime, Shanghai, China), the slices were incubated with secondary antibody (ab6789, Abcam, Cambridge, UK) for 1 h at room temperature. The 3,3′-diaminobenzidine (DAB) substrate kit (ab64238, Abcam, Cambridge, UK) was employed for staining after washing. The sections were counterstained with hematoxylin (H9627, Sigma-Aldrich, CA, USA) and examined using an optical microscope (200×; positive staining appears brown). The data were analyzed quantitatively using ImageJ software (version 1.54, National Institutes of Health, MD, USA).

Statistical Analysis

Statistical analyses were performed using GraphPad Prism 8.0 (GraphPad Software, CA, USA). Quantitative data are presented as mean ± standard deviation (SD). Normality and homogeneity of variance were assessed prior to analysis. For comparisons between two independent groups, Student's unpaired t-test was used. For comparisons among three or more independent groups, one-way analysis of variance (ANOVA) was used, followed by Tukey's multiple comparisons test for pairwise group comparisons. When comparisons were made between multiple treatment groups and a single control group, Dunnett's multiple comparisons test was applied. For experiments involving repeated measurements over time, two-way repeated measures ANOVA was used, followed by Tukey's post hoc multiple comparisons. A value of $p < 0.05$ was considered statistically significant.

Results

Network Pharmacology Predicted PTGS1 as a Potential Target of SRG

To explore the molecular targets of SRG, a network pharmacology approach was conducted (**Supplementary Table 1**). Among the 85 potential targets identified, PTGS1 was selected as a candidate for further investigation. KEGG pathway enrichment analysis revealed that SRG-related targets were significantly enriched in pathways associated with osteoclast differentiation, including the tumor necrosis factor (TNF) signaling pathway, nuclear factor kappa B (NF-κB) signaling pathway, and mitogen-activated protein kinase (MAPK) signaling pathway (**Supplementary Fig. 1** and **Supplementary Table 3**). To further validate the direct interaction between SRG and PTGS1, molecular docking was performed, and the results demonstrated that SRG exhibited favorable binding affinity for PTGS1 (**Supplementary Fig. 2**). Collectively, these results suggested that SRG may exert its anti-osteoporotic effects through PTGS1 and its downstream signaling pathways.

SRG Inhibited Osteoclast Differentiation and PTGS1 Expression

To confirm the responsiveness of RAW 264.7 cells to RANKL stimulation, NFAT2 (encoded by NFATc1) protein expression was examined. As shown in Fig. 1A,B, RANKL markedly increased NFAT2 expression (Fig. 1A,B, $p < 0.05$). TRAP staining results demonstrated that SRG significantly reduced osteoclast differentiation in a concentration-dependent manner, as indicated by the decreased reddish-purple precipitate (Fig. 1C,E, $p < 0.05$). Moreover, F-actin ring staining demonstrated that SRG diminished the formation of F-actin, indicating that SRG suppressed the bone-resorbing capacity of osteoclasts (Fig. 1D,F, $p < 0.05$). Consistently, treatment with 2.5, 5, and 10 μM SRG markedly downregulated *CTSK*, *Mmp9* and *NFATc1* in RANKL-treated RAW 264.7 cells (Fig. 2A–C, $p < 0.01$). WB analysis showed a dose-dependent decrease in COX1 (encoded by PTGS1) levels in RANKL-induced RAW 264.7 cells following SRG treatment (Fig. 2D,E, $p < 0.05$).

SRG Inhibited Osteoclast Differentiation by Suppressing PTGS1

To analyze the role of PTGS1 in SRG-mediated inhibition of osteoclast differentiation, we constructed a PTGS1 overexpression vector. QRT-PCR results revealed a significant increase in PTGS1 levels in the PTGS1 group compared to the NC group (Fig. 3A, $p < 0.001$). WB analysis further indicated that COX1 protein expression was notably increased upon PTGS1 overexpression, together with

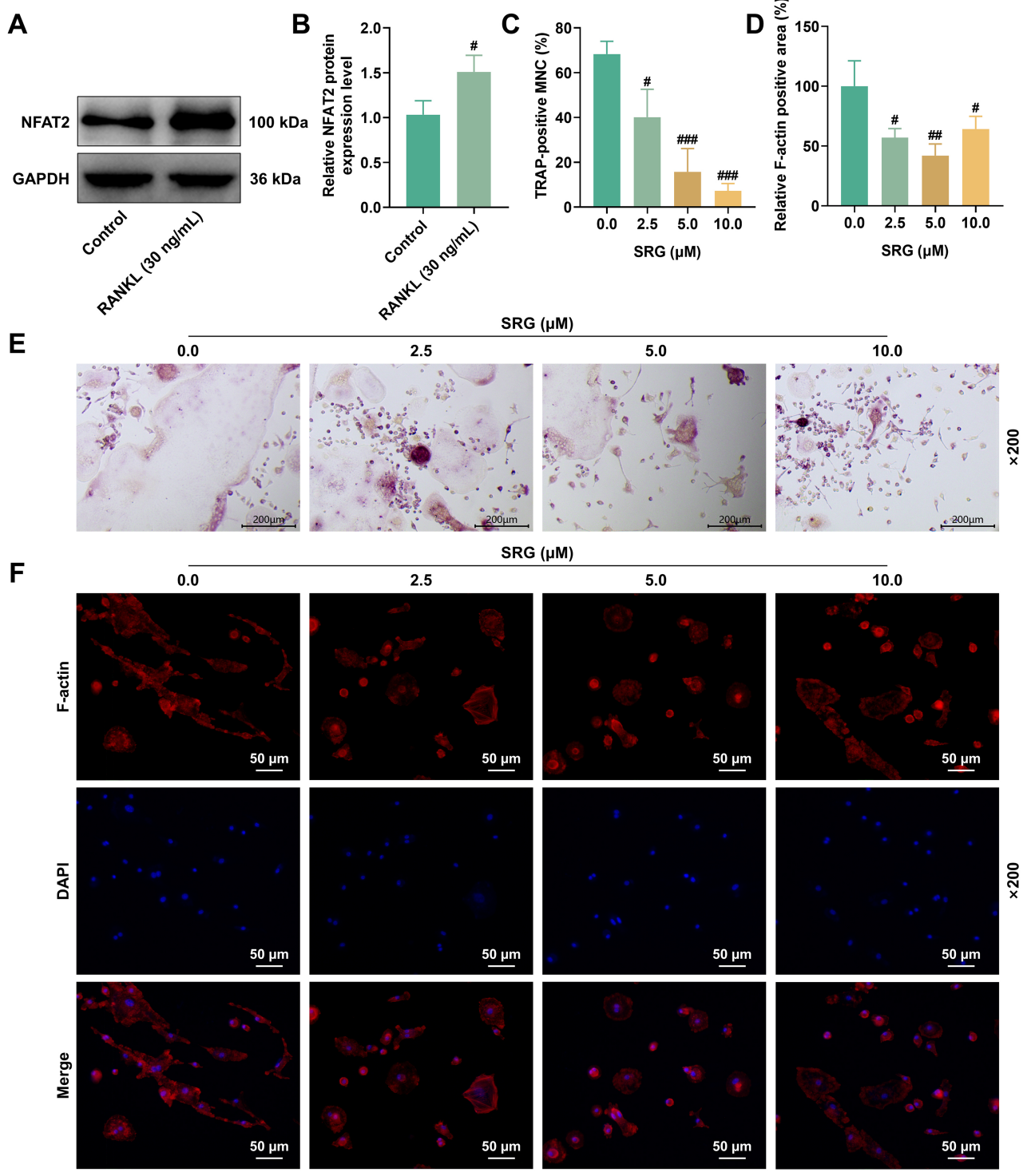

Fig. 1. Effect of syringin (SRG) on osteoclast differentiation in receptor activator of nuclear factor-κB ligand (RANKL)-induced RAW 264.7 cells. (A,B) Western blot (WB) analysis of nuclear factor of activated T cells 1 (NFATc1, also known as NFAT2) protein levels, with glyceraldehyde-3-phosphate dehydrogenase (GAPDH) as the loading control. (C,E) Tartrate-resistant acid phosphatase (TRAP) staining and quantification of TRAP-positive multinucleated cells (MNCs). Magnification: 200×, scale bar: 200 μm. (D,F) F-actin rings were observed in osteoclasts under confocal microscopy. Magnification: 200×, scale bar: 50 μm. $^{\#}p < 0.05$, $^{\#\#}p < 0.01$, $^{\#\#\#}p < 0.001$ vs. Control group or 0.

upregulated NFAT2 protein (Fig. 3B–D, $p < 0.05$). Subsequently, TRAP staining showed that SRG reduced osteoclast differentiation (reddish-purple precipitate), which was reversed by PTGS1 overexpression (Fig. 3E,F, $p <$

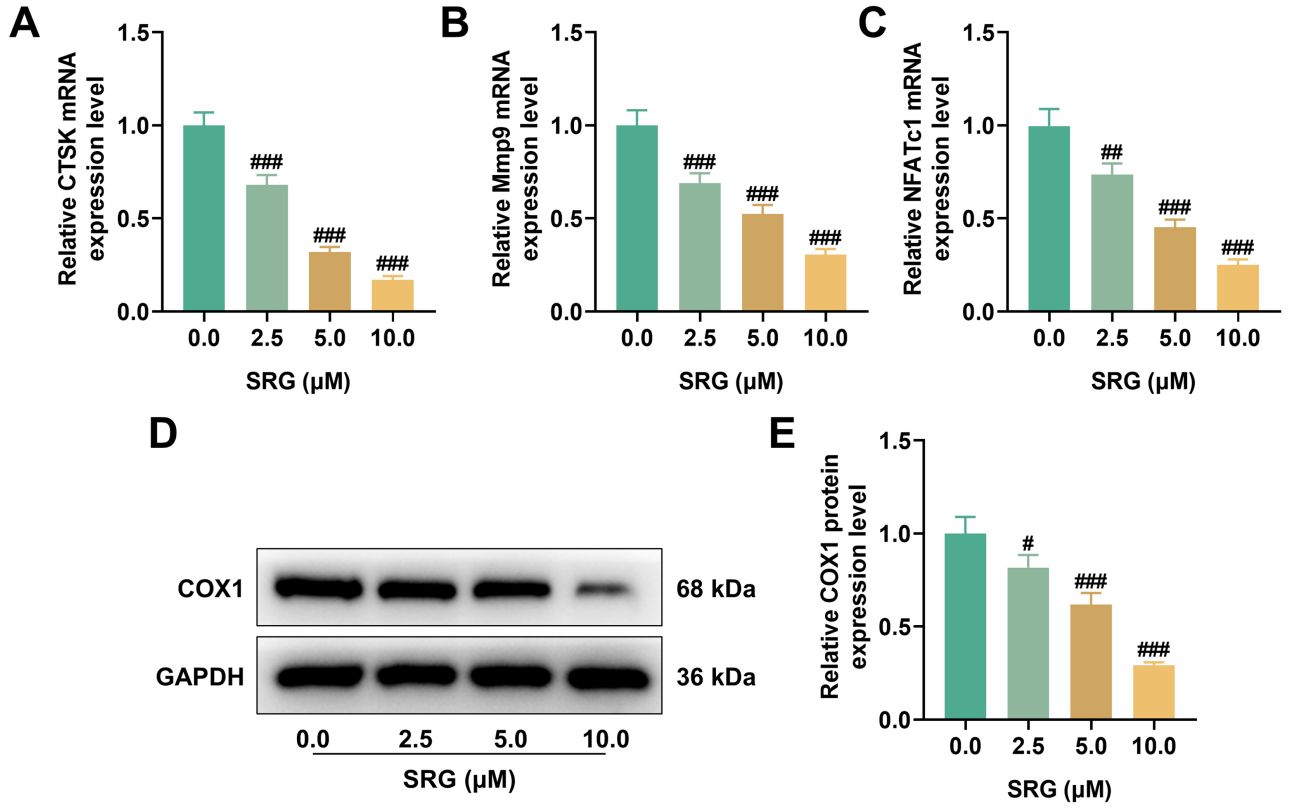

Fig. 2. SRG suppressed osteoclast-related gene and prostaglandin-endoperoxide synthase 1 (PTGS1, also known as COX1) protein expression. (A–C) Quantitative real-time polymerase chain reaction (qRT-PCR) analysis of cathepsin K (*CTSK*), matrix metalloproteinase 9 (*Mmp9*), and *NFATc1* mRNA levels in RANKL-induced RAW 264.7 cells treated with 0, 2.5, 5, and 10 μM SRG. *GAPDH* was used as the internal control. (D,E) WB analysis of COX1 protein expression, with GAPDH as the loading control. Each experiment was independently repeated three times. $^{\#}p < 0.05$, $^{\#\#}p < 0.01$, $^{\#\#\#}p < 0.001$ vs. 0.

0.05). The levels of *CTSK*, *Mmp9*, and *NFATc1* were lower in the SRG group than the control group (Fig. 3G–I, $p < 0.001$), and were higher in the SRG+PTGS1 group than the SRG+NC group (Fig. 3G–I, $p < 0.001$).

SRG Alleviated OVX-Induced Osteoporosis

The body weight of rats showed no significant changes in the E_2, SRG-L, and SRG-H groups compared with the OVX group (Fig. 4A). OVX treatment reduced uterine weight, femoral weight, and femoral density, which was partially offset by treatment with E_2, SRG-L, and SRG-H (Fig. 4B–D, $p < 0.01$). Compared with the Sham group, the OVX group presented increases in serum levels of TRAP, ALP and AST, and decreases in ALT (Fig. 4E–H, $p < 0.001$). Relative to the OVX group, the E_2, SRG-L, and SRG-H groups showed reduced serum levels of TRAP, ALP and ALT (Fig. 4E–G, $p < 0.001$), and the SRG-L and SRG-H groups exhibited downregulation of AST (Fig. 4H, $p < 0.001$). Histological analysis of the femur demonstrated that OVX treatment reduced the trabecular area (purple-stained trabecular bone) (Fig. 5A,B, $p < 0.05$), whereas E_2, SRG-L, and SRG-H interventions dramatically reversed such a decline (Fig. 5A,B, $p < 0.05$). TRAP staining showed that the OVX group exhibited a significantly higher number of osteoclasts than the Sham group (Fig. 5C,D, $p < 0.001$); however, the number of osteoclasts was substantially decreased upon E2, SRG-L, and SRG-H treatments (Fig. 5C,D, $p < 0.05$). IHC staining revealed that NFATc1, a key osteoclastogenesis marker, showed stronger brown-positive expression in the OVX group than in the sham group (Fig. 5E,F, $p < 0.001$), which was counteracted by E2, SRG-L, and SRG-H treatments (Fig. 5E,F, $p < 0.05$).

Discussion

In this study, we found that SRG treatment improves PMOP. ALP is a widely distributed enzyme primarily involved in phosphate hydrolysis and plays a significant role in bone metabolism [18]. Elevated ALP levels, secreted by osteoblasts during bone formation, typically reflect increased bone formation activity [19]. In PMOP patients, ALP serves as an important indicator of bone metabolic status [20]. Previous research identified a negative correlation between ALP levels and bone density [21,22], suggesting that elevated ALP may indicate an imbalance in the bone remodeling process. *In vivo*, we observed that

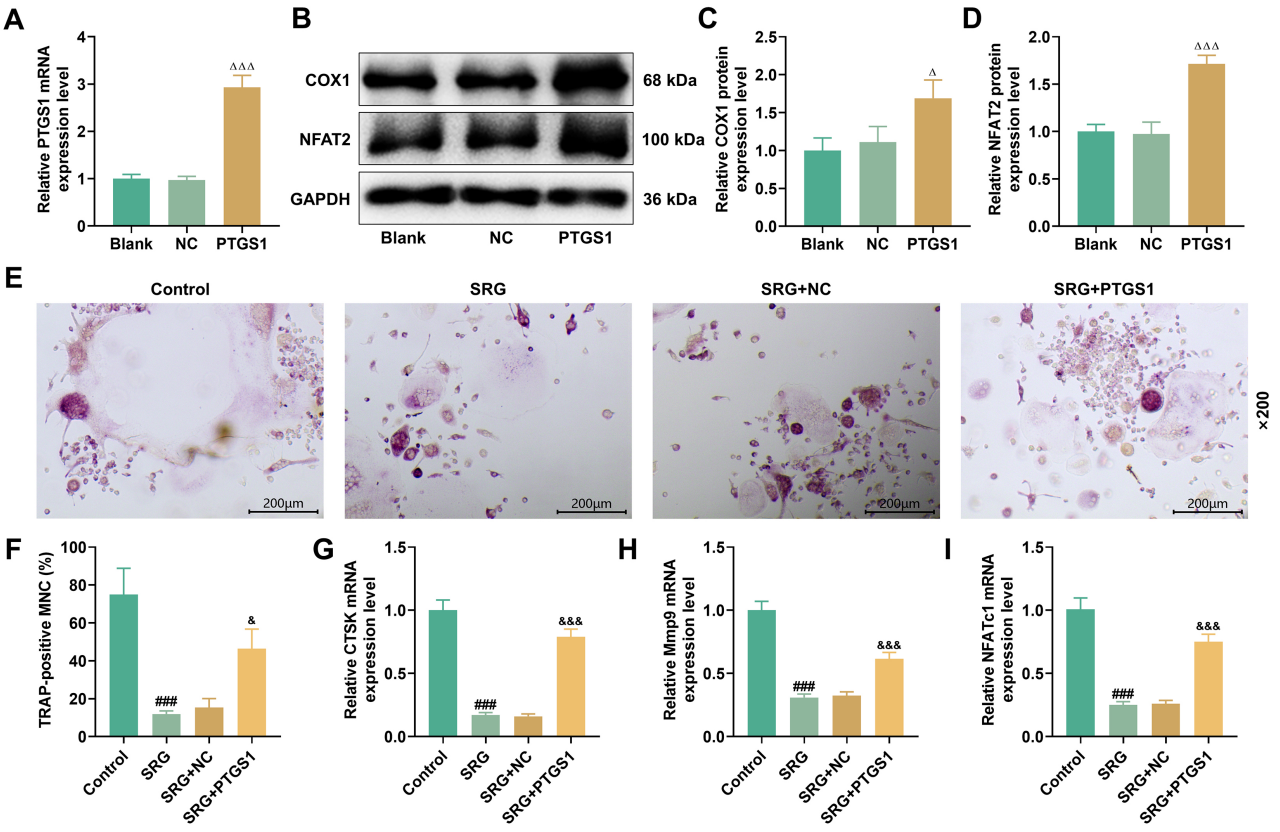

Fig. 3. SRG modulated osteoclast differentiation via PTGS1. (A) *PTGS1* mRNA expression in Blank, negative control (NC), and PTGS1 overexpression groups was analyzed by qRT-PCR. *GAPDH* served as the internal control. Blank represents untreated control cells, whereas NC represents cells transfected with the empty vector. (B–D) WB analysis was used to quantify COX1 and NFAT2 protein levels. GAPDH was used as the loading control. (E,F) TRAP staining was used to evaluate osteoclast differentiation in the Control, SRG, SRG+NC, and SRG+PTGS1 groups. TRAP-positive MNCs were counted. Magnification: 200×, scale bar: 200 μm. (G–I) QRT-PCR analysis of *CTSK*, *Mmp9*, and *NFATc1* mRNA expression. *GAPDH* was used as the internal control. Experiments were independently repeated three times. $^{###}p < 0.001$ vs. Control; $^{\Delta}p < 0.05$, $^{\Delta\Delta\Delta}p < 0.001$ vs. NC; $^{\&}p < 0.05$, $^{\&\&\&}p < 0.001$ vs. SRG+NC.

SRG attenuated the OVX-induced elevation of ALP levels. Given the close association between ALP and bone turnover, the reduction in ALP following SRG treatment may reflect suppression of excessive bone remodeling under estrogen-deficient conditions. In addition, decreased serum ALT levels were observed in OVX rats. Similar alterations in liver enzyme profiles have been reported in ovariectomized animal models and may be associated with metabolic adaptations following estrogen deficiency, including changes in hepatic lipid metabolism and systemic energy balance [18]. However, the exact biological foundation for this discovery is still unknown. Accordingly, the reduction in ALT should be interpreted with caution and should not be considered direct evidence of improved hepatic function or bone-protective effects. Importantly, SRG treatment did not induce abnormal elevations in ALT or AST levels, suggesting no obvious hepatotoxicity under the current experimental conditions. TRAP is predominantly expressed in osteoclasts and is extensively involved in bone and mineral metabolism. As a hallmark enzyme of osteoclasts, increased TRAP activity is closely related to the onset of osteoporosis. Studies have shown that TRAP plays a crucial role in promoting bone resorption by regulating the degradation of bone matrix and the release of minerals, thereby directly affecting bone structure and function [23]. Our findings demonstrated that SRG significantly inhibited TRAP levels in both osteoclast models and OVX-induced osteoporosis animal models. Taken together, SRG may alleviate PMOP by inhibiting the levels of TRAP.

We also found that SRG inhibited PTGS1 levels in osteoclasts. PTGS1, a key enzyme in prostaglandin synthesis, plays a critical role in regulating inflammatory responses and bone metabolism. Research indicated that PTGS1 inhibitors or PTGS1 silencing can significantly attenuate LPS-induced inflammatory responses through negative regulation of the NF-κB signaling pathway [24]. Inflammatory cytokines not only promote bone resorption but also disrupt the bone remodeling process, decreasing bone density and exacerbating the development of osteoporosis [25]. Additionally, the PTGS1 inhibitor BGJb has been reported to

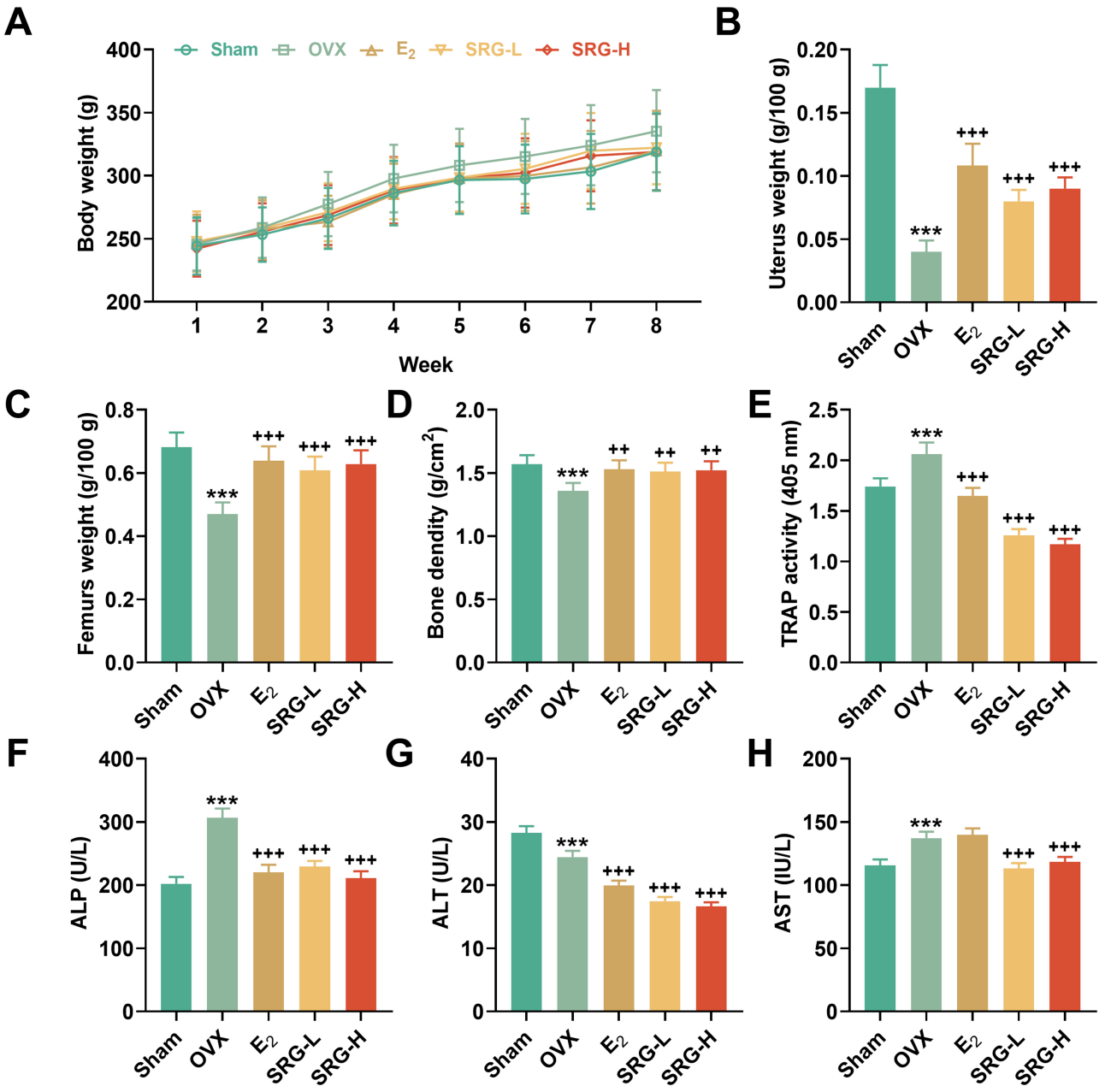

Fig. 4. Effect of SRG on body weight, organ weights, bone density, and serum biomarkers in ovariectomized (OVX) rats. (A) Body weight measurements in Sham, OVX, 17β-estradiol (E_2), SRG-low (L), and SRG-high (H) groups of rats after 8 weeks of treatment. Data are presented as mean ± standard deviation (SD), and error bars represent SD. (B,C) Analysis of uterine and femoral weights. (D) Femoral bone mineral density. (E) TRAP activity measured using a commercial kit. (F–H) Serum alkaline phosphatase (ALP), alanine aminotransferase (ALT), and aspartate aminotransferase (AST) levels measured by ELISA. n = 8 per group. $^{***}p < 0.001$ vs. Sham; $^{++}p < 0.01$, $^{+++}p < 0.001$ vs. OVX.

suppress bone resorption [26]. MMP9, a zinc-dependent protease belonging to the matrix metalloproteinase family, primarily functions to degrade extracellular matrix components, such as collagen and elastin [27]. Osteoclasts, responsible for bone resorption, secrete various enzymes, including MMP9, to degrade bone matrix [28]. Under normal physiological conditions, MMP9 activity is an integral part of the bone remodeling process, ensuring a balance between resorption and formation. However, in osteoporosis, MMP9 expression is often significantly increased, leading to enhanced bone resorption and decreased bone density [29]. A close correlation has been demonstrated between MMP9 upregulation and an elevated risk of fracture [30]. In addition, PGE2 synthesized by PTGS1 can enhance MMP9 expression [11]. Our study demonstrated that SRG reduced PTGS1 and *Mmp9* expression, and PTGS1 over-

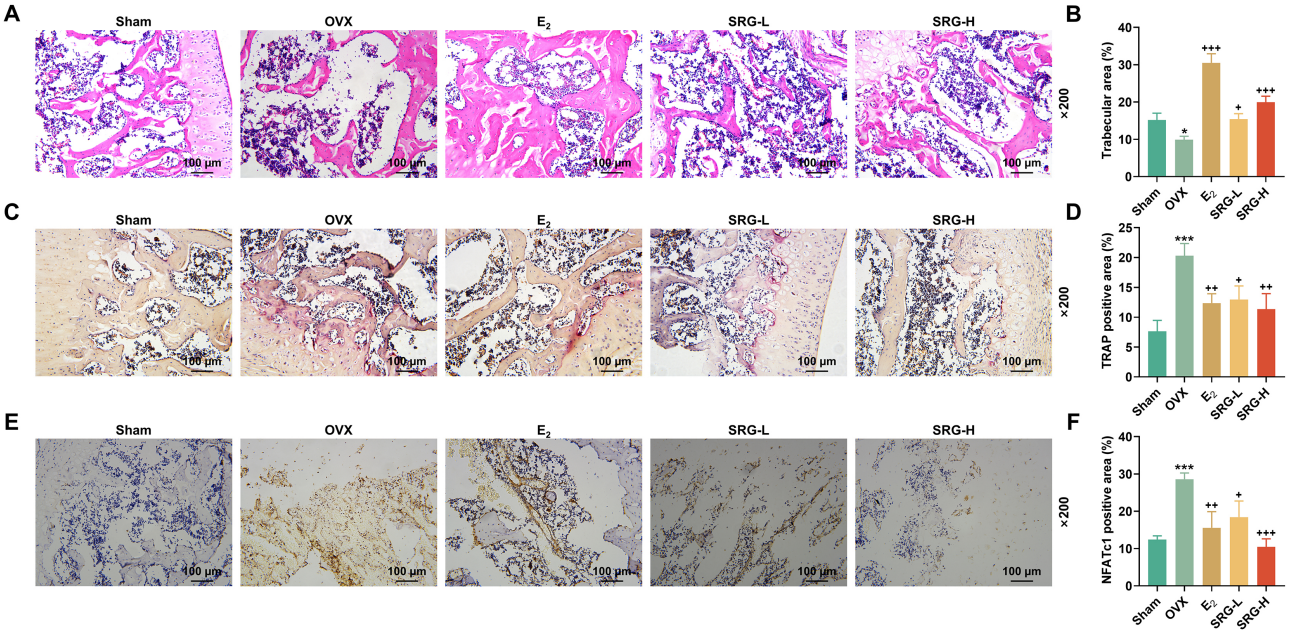

Fig. 5. SRG attenuated bone histopathological changes and osteoclast activity in OVX rats. (A,B) Hematoxylin and eosin (H&E) staining of femoral tissue. Magnification: 200×, scale bar: 100 μm. (C,D) TRAP staining to analyze osteoclast activity. Magnification: 200×, scale bar: 100 μm. (E,F) Immunohistochemical (IHC) staining of NFATc1. Magnification: 200×, scale bar: 100 μm. n = 8 per group. $^{*}p < 0.05$, $^{***}p < 0.001$ vs. Sham; $^{+}p < 0.05$, $^{++}p < 0.01$, $^{+++}p < 0.001$ vs. OVX.

expression partially reversed the inhibitory effect of SRG on *Mmp9* expression. These findings suggest a potential association between PTGS1 regulation and *Mmp9* expression during osteoclast differentiation, which may contribute to the protective effects of SRG against PMOP. However, whether PTGS1 regulates MMP9 through PGE2-dependent or independent pathways remains to be determined.

Although this study thoroughly explored the role of SRG in inhibiting osteoclast differentiation via PTGS1 regulation, several limitations should be acknowledged. First, although PTGS1 overexpression altered *Mmp9* expression, the mechanistic link between PTGS1 activity, PGE2 signaling, and *Mmp9* regulation was not directly determined. Second, the effects of SRG on osteoblast differentiation were not evaluated; changes in serum ALP levels indirectly reflect bone turnover but do not provide a direct assessment of osteogenic potential. Third, a systematic investigation of SRG dosage and treatment duration is needed to establish optimal therapeutic strategies. Future studies are warranted to address these limitations and further evaluate the translational potential of SRG for PMOP treatment.

Conclusion

In conclusion, this study demonstrates that SRG effectively inhibits osteoclast differentiation and reduces PTGS1 expression, resulting in downregulation of key osteoclastogenic markers, including *CTSK*, *Mmp9*, and *NFATc1*. PTGS1 overexpression partially reverses these effects, indicating its involvement in SRG-mediated regulation. In the OVX-induced osteoporosis rat model, SRG treatment exerts therapeutic effects against PMOP. Despite these promising findings, several limitations should be acknowledged, including the lack of direct assessment of osteoblast differentiation and incomplete elucidation of the PTGS1-PGE2-*Mmp9* mechanistic axis. Future studies are warranted to clarify these mechanisms, evaluate osteogenic effects, and optimize dosing strategies to further assess the translational potential of SRG for treating osteoporosis.

Availability of Data and Materials

The analyzed datasets generated during the study are available from the corresponding author on reasonable request.

Author Contributions

QZ and JHH designed the research study; YHY performed the research; QZ collected and analyzed the data. JHH has been involved in drafting the manuscript and all authors have been involved in revising it critically for important intellectual content. All authors gave final approval of the version to be published. All authors have participated sufficiently in the work to take public responsibility for appropriate portions of the content and agreed to be accountable for all aspects of the work in ensuring that questions related to its accuracy or integrity.

Ethics Approval and Consent to Participate

The Animal Ethics Committee of the Zhejiang Provincial Animal Center gave its approval (Approval No. ZJCLA-IACUC-20011001) to the *in vivo* tests. All procedures complied with the ARRIVE Guidelines 2.0.

Acknowledgment

Not applicable.

Funding

This work was supported by Applied Basic Research Project of Changzhou Science and Technology Bureau under Grant [number CJ20220111]; Changzhou "Longcheng Medical Star" Health Youth Scientific and Technological Talent Support Program under Grant [number lcyx2024012]; Medical Research Project of the Health Commission of Jiangsu Province under Grant [number Z2021072].

Conflict of Interest

The authors declare no conflict of interest.

Supplementary Material

Supplementary material associated with this article can be found, in the online version, at https://doi.org/10.24976/Discov.Med.202638210.181.

References

[1] Aibar-Almazán A, Voltes-Martínez A, Castellote-Caballero Y, Afanador-Restrepo DF, Carcelén-Fraile MDC, López-Ruiz E. Current Status of the Diagnosis and Management of Osteoporosis. International Journal of Molecular Sciences. 2022; 23: 9465. https://doi.org/10.3390/ijms23169465

[2] Brown JP. Long-Term Treatment of Postmenopausal Osteoporosis. Endocrinology and Metabolism (Seoul, Korea). 2021; 36: 544–552. https://doi.org/10.3803/EnM.2021.301

[3] Xu J, Yu L, Liu F, Wan L, Deng Z. The effect of cytokines on osteoblasts and osteoclasts in bone remodeling in osteoporosis: a review. Frontiers in Immunology. 2023; 14: 1222129. https://doi.org/10.3389/fimmu.2023.1222129

[4] Thapa S, Nandy A, Rendina-Ruedy E. Endocrinal metabolic regulation on the skeletal system in post-menopausal women. Frontiers in Physiology. 2022; 13: 1052429. https://doi.org/10.3389/fphys.2022.1052429

[5] Black DM, Rosen CJ. Clinical Practice. Postmenopausal Osteoporosis. The New England Journal of Medicine. 2016; 374: 254–262. https://doi.org/10.1056/NEJMcp1513724

[6] Batoon L, Millard SM, Raggatt LJ, Wu AC, Kaur S, Sun LWH, et al. Osteal macrophages support osteoclast-mediated resorption and contribute to bone pathology in a postmenopausal osteoporosis mouse model. Journal of Bone and Mineral Research : the Official Journal of the American Society for Bone and Mineral Research. 2021; 36: 2214–2228. https://doi.org/10.1002/jbmr.4413

[7] Fischer V, Haffner-Luntzer M. Interaction between bone and immune cells: Implications for postmenopausal osteoporosis. Seminars in Cell & Developmental Biology. 2022; 123: 14–21. https://doi.org/10.1016/j.semcdb.2021.05.014

[8] Zhao Y, Luo X, Hu J, Panga MJ, Appiah C, Du Z, et al. Syringin alleviates bisphenol A-induced spermatogenic defects and testicular injury by suppressing oxidative stress and inflammation in male zebrafish. International Immunopharmacology. 2024; 131: 111830. https://doi.org/10.1016/j.intimp.2024.111830

[9] Shi Z, Zou S, Shen Z, Luan F, Yan J. High-throughput metabolomics using UPLC/Q-TOF-MS coupled with multivariate data analysis reveals the effect and mechanism of syringin against ovariectomized osteoporosis. Journal of Chromatography. B, Analytical Technologies in the Biomedical and Life Sciences. 2021; 1183: 122957. https://doi.org/10.1016/j.jchromb.2021.122957

[10] Ren X, Zhu Y, Xie L, Zhang M, Gao L, He H. Yunnan Baiyao diminishes lipopolysaccharide-induced inflammation in osteoclasts. Journal of Food Biochemistry. 2020; 44: e13182. https://doi.org/10.1111/jfbc.13182

[11] Miralles M, Wester W, Sicard GA, Thompson R, Reilly JM. Indomethacin inhibits expansion of experimental aortic aneurysms via inhibition of the cox2 isoform of cyclooxygenase. Journal of Vascular Surgery. 1999; 29: 884–884–892; discussion 892–893. https://doi.org/10.1016/s0741-5214(99)70216-8

[12] Phromnoi K, Yodkeeree S, Pintha K, Mapoung S, Suttajit M, Saenjum C, et al. Anti-Osteoporosis Effect of *Perilla frutescens* Leaf Hexane Fraction through Regulating Osteoclast and Osteoblast Differentiation. Molecules (Basel, Switzerland). 2022; 27: 824. https://doi.org/10.3390/molecules27030824

[13] Kats A, Norgård M, Wondimu Z, Koro C, Concha Quezada H, Andersson G, et al. Aminothiazoles inhibit RANKL- and LPS-mediated osteoclastogenesis and PGE2 production in RAW 264.7 cells. Journal of Cellular and Molecular Medicine. 2016; 20: 1128–1138. https://doi.org/10.1111/jcmm.12814

[14] Zhao D, Liu K, Wang J, Shao H. Syringin exerts anti-inflammatory and antioxidant effects by regulating SIRT1 signaling in rat and cell models of acute myocardial infarction. Immunity, Inflammation and Disease. 2023; 11: e775. https://doi.org/10.1002/iid3.775

[15] Zhao F, Maren NA, Kosentka PZ, Liao YY, Lu H, Duduit JR, et al. An optimized protocol for stepwise optimization of real-time RT-PCR analysis. Horticulture Research. 2021; 8: 179. https://doi.org/10.1038/s41438-021-00616-w

[16] Zhao Y, Xu Y, Zheng H, Lin N. QingYan formula extracts protect against postmenopausal osteoporosis in ovariectomized rat model via active ER-dependent MEK/ERK and PI3K/Akt signal pathways. Journal of Ethnopharmacology. 2021; 268: 113644. https://doi.org/10.1016/j.jep.2020.113644

[17] Kim M, Kim HS, Kim JH, Kim EY, Lee B, Lee SY, et al. Chaenomelis fructus inhibits osteoclast differentiation by suppressing NFATc1 expression and prevents ovariectomy-induced osteoporosis. BMC Complementary Medicine and Therapies. 2020; 20: 35. https://doi.org/10.1186/s12906-020-2841-9

[18] Cheng X, Zhao C. The correlation between serum levels of alkaline phosphatase and bone mineral density in adults aged 20 to 59 years. Medicine. 2023; 102: e34755. https://doi.org/10.1097/MD.0000000000034755

[19] Ansari S, Ito K, Hofmann S. Alkaline Phosphatase Activity of Serum Affects Osteogenic Differentiation Cultures. ACS Omega. 2022; 7: 12724–12733. https://doi.org/10.1021/acsomega.1c07225

[20] Migliorini F, Maffulli N, Spiezia F, Tingart M, Maria PG, Riccardo G. Biomarkers as therapy monitoring for postmenopausal osteoporosis: a systematic review. Journal of Orthopaedic Surgery and Research. 2021; 16: 318. https://doi.org/10.1186/s13018-021-02474-7

[21] Shu J, Tan A, Li Y, Huang H, Yang J. The correlation between serum total alkaline phosphatase and bone mineral density in young adults. BMC Musculoskeletal Disorders. 2022; 23: 467. https://doi.org/10.1186/s12891-022-05438-y

[22] Rai AD, Sherpa ML, Singh A, Thejaswi SG, Bhutia RD. Bone Alkaline Phosphatase and Urine Hydroxyproline Assay in Pre and Postmenopausal Women in the State of Sikkim and its Correlation with Bone Mineral Density. Journal of Mid-life Health. 2021; 12: 304–309. https://doi.org/10.4103/jmh.jmh_73_21

[23] Šromová V, Sobola D, Kaspar P. A Brief Review of Bone Cell Function and Importance. Cells. 2023; 12: 2576. https://doi.org/10.3390/cells12212576

[24] Wang Y, Liu Y, Zhang M, Lv L, Zhang X, Zhang P, et al. Inhibition of PTGS1 promotes osteogenic differentiation of adipose-derived stem cells by suppressing NF-kB signaling. Stem Cell Research & Therapy. 2019; 10: 57. https://doi.org/10.1186/s13287-019-1167-3

[25] Umur E, Bulut SB, Yiğit P, Bayrak E, Arkan Y, Arslan F, et al. Exploring the Role of Hormones and Cytokines in Osteoporosis Development. Biomedicines. 2024; 12: 1830. https://doi.org/10.3390/biomedicines12081830

[26] Allison AC, Chin RC, Cheng Y. Cyclooxygenase inhibitors vary widely in potency for preventing cytokine-induced bone resorption. Annals of the New York Academy of Sciences. 1993; 696: 303–306. https://doi.org/10.1111/j.1749-6632.1993.tb17165.x

[27] Rashid ZA, Bardaweel SK. Novel Matrix Metalloproteinase-9 (MMP-9) Inhibitors in Cancer Treatment. International Journal of Molecular Sciences. 2023; 24: 12133. https://doi.org/10.3390/ijms241512133

[28] Kou L, Jiang X, Lin X, Huang H, Wang J, Yao Q, et al. Matrix Metalloproteinase Inspired Therapeutic Strategies for Bone Diseases. Current Pharmaceutical Biotechnology. 2021; 22: 451–467. https://doi.org/10.2174/1389201021666200630140735

[29] Liu YY, Ding YF, Sui HJ, Liu W, Zhang ZQ, Li F. Pilose antler (Cervus elaphus Linnaeus) polysaccharide and polypeptide extract inhibits bone resorption in high turnover type osteoporosis by stimulating the MAKP and MMP-9 signaling pathways. Journal of Ethnopharmacology. 2023; 304: 116052. https://doi.org/10.1016/j.jep.2022.116052

[30] Pham TM, Erichsen JL, Kowal JM, Overgaard S, Schmal H. Elevation of Pro-Inflammatory Cytokine Levels Following Intra-Articular Fractures-A Systematic Review. Cells. 2021; 10: 902. https://doi.org/10.3390/cells10040902